RESEARCH ARTICLE | FEBRUARY 01 2002

Xenon charge exchange cross sections for electrostatic thruster models

J. Scott Miller; Steve H. Pullins; Dale J. Levandier; Yu-hui Chiu; Rainer A. Dressler

J. Appl. Phys. 91, 984–991 (2002)
https://doi.org/10.1063/1.1426246

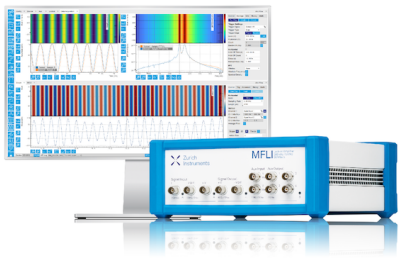

Xenon charge exchange cross sections for electrostatic thruster models

J. Scott Miller[a] and Steve H. Pullins
Air Force Research Laboratory, Space Vehicles Directorate, Hanscom AFB, Massachusetts 01731-3010

Dale J. Levandier and Yu-hui Chiu
Boston College, Institute for Scientific Research, Newton, Massachusetts 02159

Rainer A. Dressler[b]
Air Force Research Laboratory, Space Vehicles Directorate, Hanscom AFB, Massachusetts 01731-3010

(Received 20 June 2001; accepted for publication 16 October 2001)

Charge exchange between xenon ions and xenon atoms is the source of a detrimental low energy plasma in the vicinity of electrostatic spacecraft thrusters. Proper modeling of charge-exchange induced spacecraft interactions requires knowledge of the respective charge-exchange cross sections. Guided-ion beam measurements and semiclassical calculations are presented for xenon atom charge-exchange collisions with Xe^+ and Xe^{2+} at energies per ion charge ranging from 1 to 300 eV. The present measurements for the symmetric $Xe^+ + Xe$ exchange system are in good agreement with several earlier experimental studies and semiclassical calculations based on the most recently computed Xe_2^+ interaction potentials. The cross sections are ~30% higher than predictions by the Rapp and Francis model [D. Rapp and W. E. Francis, J. Chem. Phys. **37**, 2631 (1962)]. The present $Xe^{2+} + Xe$ symmetric charge exchange measurements are the first to cover the ion energy range from 40 to 600 eV. The cross sections are in good agreement with low-energy drift tube measurements and are significantly lower than previous higher energy measurements. A simple model for symmetric two-electron transfer is proposed that is in good agreement with the present measurements. The onset for the asymmetric charge-exchange process, $Xe^{2+} + Xe \rightarrow 2Xe^+$, is observed to be at 10 eV. For this process, a cross section of $2.8 \pm 0.9\ \text{Å}^2$ is measured for a Xe^{2+} energy of 600 eV. © *2002 American Institute of Physics.* [DOI: 10.1063/1.1426246]

I. INTRODUCTION

Electrostatic spacecraft thrusters, most notably ion and Hall effect thrusters (HETs), offer substantial propulsion system weight savings. In parallel with recent successful deployments of these electric propulsion engines, for example ion thrusters on Deep-Space 1,[1] there have been intensified research and development efforts to broaden their mission range. The development is heavily dependent on a concerted test and modeling program. Thruster modeling is particularly necessary to extrapolate test observations, mostly conducted in ground-based facilities, to space environmental conditions, which are not adequately reproduced in current test vacuum chambers.

A key problem in designing a propulsion system for a particular satellite is predicting the impact of thruster exhaust on spacecraft subsystems such as solar arrays and instrumentation. In electrostatic thrusters, a propellant is efficiently ionized in a confined discharge, and the ions are accelerated to energies between 0.2 eV and 1 keV. In ion thrusters, the acceleration field is generated with grids, while in HET thrusters, the acceleration occurs in a coaxial discharge chamber with an external hollow cathode. The propellant of choice is xenon because it can be ionized very efficiently, and because its high atomic mass provides high thrust levels. A primary hazard of electrostatic thrusters is the generation of low-energy charge-exchange ions that are produced in collisions between accelerated ions and the unionized propellant atoms. These ions wander out of the main ion beam of the thruster and are picked up either by weaker ambient fields, or by the acceleration fields, after which they can be directed at sensitive spacecraft surfaces. Charge-exchange ions are the primary source of ion thruster grid-erosion[2] and could potentially lead to failure of solar arrays due to ion sputtering by return-flux ions.[3]

The design of future spacecraft with electrostatic propulsion thrusters must include a detailed modeling effort that predicts return-flux ion currents attributable to charge-exchange ions. The return-flux ion currents are directly proportional to the charge-exchange cross sections that lead to low-energy ions. There has been considerable uncertainty in the thruster modeling community with respect to the size of these cross sections. Earlier models of ion thrusters[3–5] have used the predictions of the Rapp and Francis model[6] for the $Xe^+ + Xe$ symmetric charge-exchange (SCX) system. Others[7,8] have referred to the more recent calculations by Sakabe and Izawa,[9] which are significantly higher. Interestingly, these calculations are also higher than the existing measurements,[10–15] which amongst themselves also exhibit significant discrepancies. Meanwhile, only low (<20 eV)[16,17] and high (>500 eV)[18,19] energy measurements of the symmetric $Xe^{2+} + Xe$ system exist, leaving out the crucial intermediate region. It is worth noting that extrapolation of the high-energy data by Hasted and Hussein[18] to low energies

[a]NRC postdoctoral fellow.
[b]Electronic mail: rainer.dressler@hanscom.af.mil

leads to substantially higher low-energy cross sections than those observed by Okuno *et al.*[16] and Koizumi *et al.*[17] Hasted and Hussain[18] have also reported the only asymmetric charge exchange cross sections for $Xe^{2+}+Xe$ (single electron transfer) at energies relevant for electrostatic thrusters. Asymmetric (nonresonant) charge exchange of multiply charged ions and neutrals are a source of ions with energies exceeding $V_{acc}\times q$, where V_{acc} is the nominal acceleration voltage of the thruster and q is the charge of the ion.[20,21]

Prior experimental studies of SCX cross sections have involved crossed and merged beam and beam cell experiments.[22] The accuracy of these ion beam techniques has been limited by either poor collection of large-angle scattered ions, poorly defined target gas densities, or poorly defined overlap between primary and target beams. These problems have been overcome by the guided-ion beam (GIB) technique developed by Teloy and Gerlich.[23,24] In a GIB experiment, the ion beam is confined by a cylindrical ion trap consisting of a radio-frequency octopole which guides the ions through the collision cell. The guiding fields ensure complete collection of both scattered primary and secondary ions. Over the years, the GIB technique has become the method of choice for determining integral nonsymmetric charge-transfer cross sections at hyperthermal energies, including the difficult hyperthermal energy range from thermal energies, traditionally studied by flowing afterglow or ICR techniques,[25] to 10 eV, below which traditional ion beam experiments have substantial sensitivity losses.

We have recently demonstrated[26] that symmetric charge-exchange cross sections

$$A^{q+}(\text{fast})+A(\text{thermal})\rightarrow A(\text{fast})+A^{q+}(\text{near-thermal}), \quad (1)$$

where A represents an atom, and q is an integer representing the charge state of the ion, can be measured with superior accuracy using the GIB technique. We established the methodology covering an energy range from 0.2 to 300 eV by measuring $Ar^+ + Ar$ cross sections, a system that has been extensively studied over the years.[9] In that work, we also identified some errors in the one-electron model of Rapp and Francis[6] that cause the predictions to be too low. Our measurements are in excellent agreement with our own semiclassical calculations of cross sections using the most recent *ab initio* potentials of Ar_2^+ calculated by Gadea and Paiderová.[27]

In the present work, we present a complete set of GIB measurements of Xe^+ and Xe^{2+} charge-exchange collisions with Xe atoms at laboratory ion energies per charge, E/q, ranging from 1 to 300 eV. In the present measurements, given the application of interest, we assume that SCX reactions produce ions with axial laboratory energies below 1 eV. The relative difference between this de-facto differential cross section and the actual SCX cross section becomes significant at the lowest ion energies studied in this work, where large-angle scattering is more important. The present measurements also pay particular attention to the electron energy used to produce the primary ions in an electron impact ion source. While the average electron energy that produces Xe^+ ions in an electrostatic thruster most likely produces ions with a statistical spin-orbit state population ratio, the broad distribution of electron energies that are responsible for producing Xe^{2+}, assuming that these ions are produced by the tail of the electron energy distribution in the discharge, is likely to produce a number of low-lying metastable electronic states of the doubly-charged ion. Semiclassical calculations based on quantum chemical potentials of Xe_2^+ and approximate expressions for the exchange interaction are also presented. As in the previous $Ar^+ + Ar$ study, the calculated cross sections for $Xe^+ + Xe$ are in good agreement with the GIB measurements, lending confidence in both theory and experiment. However, the application of exchange energies derived from spin-orbit potentials to calculate spin-orbit state-selected cross sections leads to spin-orbit state cross section ratios in disagreement with present measurements as well as earlier work, implying that improved quantum chemical calculations are necessary to provide more accurate long-range potentials of Xe_2^+.

II. EXPERIMENT

The instrument used for the cross section measurements has been described in detail previously,[28,29] and will only be discussed briefly here. A beam of Xe^+ is produced by electron impact ionization just outside of an effusive nozzle backed with 99.999% Xe. The ion beam is accelerated into a Wien velocity filter for mass selection, and then decelerated and focused into a system of two tandem rf octopole ion guides. The primary ion beam energy is reduced to approximately 0.2 eV in the injection region in order to minimize transverse velocity components and the associated rf heating of the ions. The present experiment has an ion energy resolution of 0.2 eV full width at half maximum (FWHM). The first octopole guides the ions through a cell which contains the collision gas at low pressures (~0.2 mTorr) in order to ensure a single-collision environment for the passing ions. The second octopole lies in series with the first and at the exit end of the collision cell. This octopole has an equal rf phase to the first, but is maintained either at a slightly lower (time-of-flight and mass spectral measurement) or 1 V higher dc bias (attenuation measurement). Ions exiting the second octopole are extracted by an electrostatic lens, which focuses and accelerates the ions into a quadrupole mass filter. Following mass analysis, the ions are detected with a channel electron multiplier.

Two methods are used to measure SCX cross sections. In the first, an attenuation experiment, a second octopole dc bias potential that is 1 V higher than the first octopole bias potential (from here on referred to as the blocking potential) prevents ions produced in the collision cell region (first octopole) that have nascent axial laboratory energies less than 1 eV from entering and passing the second octopole. The attenuation of the primary ion beam experienced when introducing the target gas into the cell then provides the measure of the cross section using following expression for single-collision conditions:

$$\sigma=\frac{I_0-I_a}{I_0 n \ell}, \quad (2)$$

where I_0 is the primary ion current, I_a is the attenuated ion current, n is the target gas density, and ℓ is the effective path length.

In the second method, time-of-flight (TOF), the experiment is operated in a pulsed mode and the primary and charge-transfer ions are distinguished by their separate arrival times. In this mode, the second octopole bias potential is ~0.4 V below the first octopole bias. The time-integrated secondary and primary signals then provide the cross section. For the nonresonant $Xe^{2+}+Xe \rightarrow 2Xe^{+}$ reaction, the quadrupole mass filter is set to a mass-scanning mode and the primary Xe^{2+} ions and the product Xe^{+} ion currents are discriminated with respect to their different mass-to-charge (m/q) ratios. The cross sections for the TOF and mass scan modes are then determined by the expression (assumes single collision conditions)

$$\sigma_i = \frac{I_i}{(I_a + \Sigma_i I_i) n \ell}, \tag{3}$$

where I_i is the secondary ion current for channel i. Additionally, this cross section is corrected by subtracting the result from one in which no target gas is admitted to the cell to give the true cross section. This is necessary in order to account for backgrounds such as charge-exchange ions produced outside of the collision cell due to background gas ($<10^{-6}$ Torr in the present experiments).

The first ionization potential (IP) of Xe is 12.13 eV[30] for producing the ground-state $5p^5(^2P_{3/2})$ ion. The excited spin-orbit component ($^2P_{1/2}$) of the $5p^5$ configuration lies 1.306 eV above the $^2P_{3/2}$ component. The energy halfwidth of the electron beam in our ionization source is on the order of 0.5 eV, and, therefore, discrimination between the two low-lying spin-orbit components is tenuous. This difficulty will be illustrated later in the discussion of the effect of the ion source electron energy on the SCX cross sections. A manifold of 16 excited states of Xe^{+} begins at 23.40 eV and continues to 28.69 eV above the ground state of neutral Xe. Therefore, when the electron energy is set to 15 eV in these experiments, Xe^{+} ions are only produced in the lowest $^2P_{3/2,1/2}$ states. The second IP of Xe lies 33.11 eV[30] above the ground state of Xe. We only obtain sufficient beam intensities above electron energies of 36 eV. The observed cross sections do not change between 36 and 40 eV. The Xe^{2+} measurements are consequently recorded with 40 eV electrons. This signifies that the beam includes important contributions from the metastable ^1D and ^1S states which have ionization energies of 35.3 and 37.6 eV, respectively.[31] Given their low excitation energies with respect to ground state $Xe^{2+}(^3P)$, it can be assumed that the Xe^{2+} ions formed in a thruster have similar distributions to those of our experiment.

III. CALCULATIONS

The $Xe^{+}+Xe$ cross-section measurements are backed up by semiclassical calculations based on the long-range potentials of the Xe_2^{+} system obtained from the literature. According to semiclassical theory and the impact parameter approximation, the SCX cross section can be expressed as

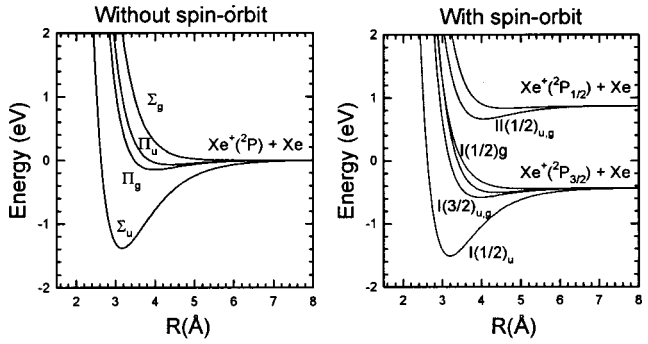

FIG. 1. Xe_2^{+} potentials with and without spin-orbit coupling as calculated by Amarouche *et al.* (see Ref. 34).

$$\sigma^{SCX} = 2\pi \int_0^{\infty} P(b) b\, db, \tag{4}$$

where σ^{SCX} is the integral SCX cross section, b is the collision impact parameter, and $P(b)$ is the charge-exchange probability. The latter can be described by[32]

$$P(b) = \sum_l g_l \sin^2 \Delta_l, \tag{5}$$

where Δ_l is the difference in elastic scattering phase shifts for trajectories on the gerade (g) and ungerade (u) interaction potentials of the charge-exchange pairs of symmetry, l, and g_l is a statistical factor. The calculation of the symmetric exchange cross section is thus reduced to knowledge of the (g,u) interaction potential pairs that have ground atomic state asymptotic limits, and the determination of the elastic scattering phase shifts according to standard means.[33]

Figure 1 displays the Xe_2^{+} interaction potentials determined by Amarouche and co-workers using a semi-empirical approach.[34] We have chosen these potentials as a starting point since the authors provide analytical expressions for them. Calculations based on *ab initio* potentials[35,36] have also been carried out and will be included in the discussion of the results. Note that a xenon ion encountering a xenon atom can propagate on 1 of 4 possible potentials in the spin-orbit free description. Charge exchange interaction occurs between states of equal electronic angular momentum (symmetry), Λ (i.e., Σ–Σ and Π–Π transitions are allowed). Spin-orbit potentials are obtained from the spin-orbit free sets using the semi-empirical approach of Cohen and Schneider that assumes that the spin-orbit interaction is independent of the internuclear distance, R.[37] This results in six potentials, four correlated with ground-state reactants, $Xe^{+}(^2P_{3/2})+Xe$, and two correlated with spin-orbit excited reactants, $Xe^{+}(^2P_{1/2})+Xe$.

In accordance with Eq. (5), the total SCX cross sections can be obtained from the spin-orbit free potentials (Fig. 1, left panel) using

$$\sigma^{SCX} = \tfrac{2}{3}\sigma_{\Pi} + \tfrac{1}{3}\sigma_{\Sigma}, \tag{6}$$

where σ_{Π} and σ_{Σ} are the cross sections for exchange when the collision system undergoes Π and Σ exchange, respectively [i.e., the phase shift difference in Eq. (5) is calculated

for the respective Π and Σ (u,g) pairs]. Cross sections for spin-orbit state-selected ions can be calculated using the spin-orbit potentials

$$\sigma_{3/2}^{\mathrm{SCX}} = \tfrac{1}{2}\{\sigma[I(1/2)u \leftrightarrow I(1/2)g] + \sigma[I(3/2)g \leftrightarrow I(3/2)u]\} \quad (7)$$

$$\sigma_{1/2}^{\mathrm{SCX}} = \sigma[II(1/2)u \leftrightarrow II(1/2)g], \quad (8)$$

where the transition probabilities [Eq. (5)] are calculated for the spin-orbit potential pairs in the square brackets. Assuming a statistical population of the reactant $Xe^{+2}P_{3/2}$ and $^2P_{1/2}$ spin-orbit states, the spin-orbit averaged cross section is then given by

$$\sigma^{\mathrm{SCX}} = \tfrac{2}{3}\sigma_{3/2}^{\mathrm{SCX}} + \tfrac{1}{3}\sigma_{1/2}^{\mathrm{SCX}}. \quad (9)$$

Johnson[38] has provided an approximate approach from which the state-selected cross sections can be obtained directly from the spin-orbit free potentials using following expressions for the charge-exchange probabilities

$$P_{3/2}(b) = \tfrac{1}{2}\sin^2\Delta_{\Pi} + \tfrac{1}{2}\sin^2[\tfrac{1}{3}(\Delta_{\Pi} + 2\Delta_{\Sigma})] \quad (10)$$

$$P_{1/2}(b) = \sin^2[\tfrac{1}{3}(\Delta_{\Sigma} + 2\Delta_{\Pi})]. \quad (11)$$

As shown in the following section, application of Eqs. (7) and (8) or (10) and (11) leads to essentially the same result for a particular set of spin-orbit free potentials.

From the size of the SCX cross sections at the ion energies of interest in this work, it becomes quickly apparent that the cross sections are governed by the potentials at long range at interatomic distances exceeding 4 Å. The interaction potentials, $V_{g,u}(R)$, can then be approximated by the combination of an ion-induced dipole potential and the exchange interaction

$$V_{g,u}(R) = -\frac{\alpha}{2R^4} \pm \frac{A}{2}\exp(-aR), \quad (12)$$

where α is the polarizability of the neutral target atom (4.044 $Å^3$)[30] and $\Delta V(R) = V_g - V_u = A\exp(-aR)$ is the R-dependent exchange energy, where A and a are parameters. Using the exponential form of Eq. (12) considerably simplifies the numerical procedure to determine the phase shift difference for conditions at which straight-line trajectories can be assumed.[26,39] In a straight-line trajectory calculation, the first term in Eq. (12) is neglected.

Potentials for Xe_2^{2+} are not known to us. For SCX cases of singly charged systems where potentials are not known, Rapp and Francis have provided an empirical expression for $\Delta V(R)$:

$$\Delta V_{\mathrm{RF}}(R) = 2IR\exp(-\alpha_I R), \quad (13)$$

where I is the ionization potential of the parent gas atom and $\alpha_I = (2I)^{1/2}$. Thus, the coupling can be estimated solely from the ionization energy of the neutral target atom. In our previous work, we have pointed out that this expression, based on a 1-electron linear combination of hydrogenic atomic orbitals (LCAO) approach, is incorrect and that the LCAO approach is more precisely represented by[26]

$$\Delta V_{\mathrm{LCAO}}(R) = \tfrac{8}{3}IR\exp(-\alpha_I R). \quad (14)$$

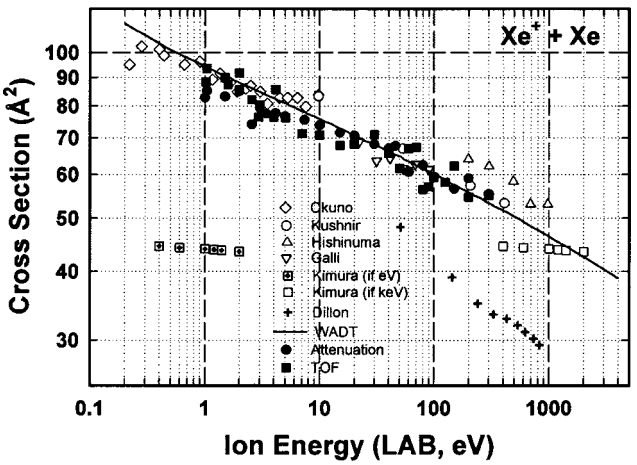

FIG. 2. $Xe^+ + Xe$ symmetric charge-exchange cross sections as a function of laboratory ion energy. The present measurements, solid circles (attenuation) and squares (TOF), are compared with previous measurements and calculations. Note that we plot Kimura and Watanabe's (see Ref. 12) calculations twice given our suspicion that the original paper provided cross sections on an electron-volt scale rather than a kilo-electron-volt scale. The solid line is a semiclassical calculation based on the potentials of Wadt (see Ref. 36).

A more rigorous treatment based on polarization perturbation theory applied to H_2^+ yields a minor correction for the asymptotic form[40,41]

$$\Delta V(R) = +\frac{8}{e}IR\exp(-\alpha_I R). \quad (15)$$

The SCX measurements for both singly and doubly charged xenon will be compared with predictions using the approximate expressions for the exchange energy. So far, the 1-electron approach to estimating the exchange energy has only been suggested for singly charged SCX systems. Here, we suggest that for doubly charged systems, the exchange energy can be estimated by setting I equal to the ionization energy required to remove two electrons from the target atom.

IV. RESULTS AND DISCUSSION

A. $Xe^+ + Xe$

Figure 2 compares the present measurements in the laboratory ion energy range of 1–300 eV with calculations and earlier measurements. The solid circles depict the present cross sections determined using the attenuation method. A blocking potential of 1 eV is applied except for the lowest energy point (1 eV LAB), where the difference between second and first octopole was set to 0.5 eV. The solid squares are present results using the TOF method. Given the potential sources of discrimination, it can be stated that, except at the lowest energies, the attenuation mode represents an upper limit to the cross sections because discrimination is primarily due to losses of primary ions scattered at large angles, thus artificially raising the cross section. At the lowest ion energies, large-angle scattering of charge-exchange ions can lead to significant laboratory energies and thus unwanted transmission of the charge-exchange ions, thereby reducing the effective cross section. Meanwhile, the lower transverse en-

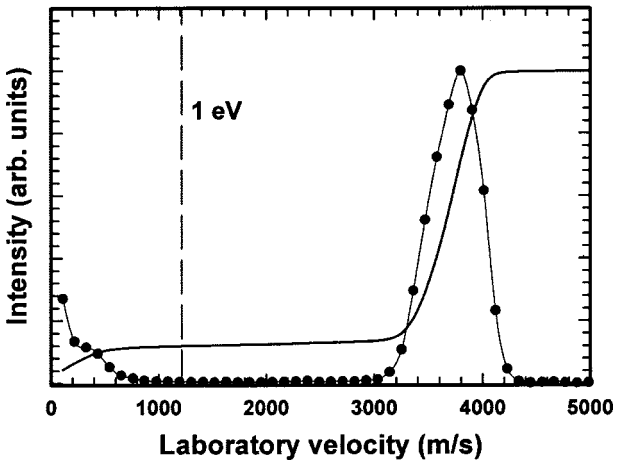

FIG. 3. Velocity transformed TOF spectrum of Xe^+ scattered on Xe at 10 eV (LAB). The solid line is the integrated spectrum. The dashed line represents the laboratory velocity corresponding to 1 eV.

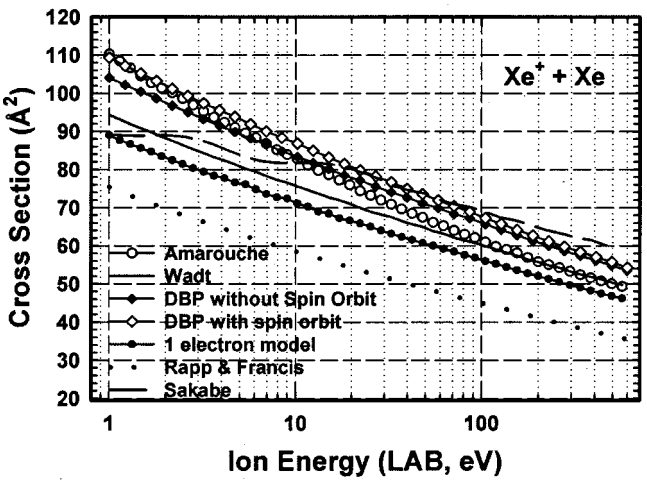

FIG. 4. Comparison of present semiclassical calculations based on existing Xe_2^+ potentials with the Rapp and Francis model predictions (see Ref. 6) and the calculations by Sakabe and Izawa (see Ref. 9). The semiclassical calculations based on the potentials of Wadt are a good representation of the present measurements.

ergies at low energies result in smaller discrimination effects. The TOF measurements, on the other hand, risk discriminating with respect to the secondary ions, either due to the poor collection of large-angle scattered charge-exchange ions, or due to the trapping of very slow ions at surface potential barriers of the first octopole. Thus, they can be regarded as lower limits to the actual cross section. Figure 3 is an example of a velocity-transformed TOF spectrum recorded at an ion energy of 10 eV. The high-energy band corresponds to the attenuated primary ion beam, the width of which is primarily governed by the TOF resolution. The low-energy band is attributable to charge-exchange ions. The solid line is the integrated intensity. The dashed line indicates the laboratory velocity corresponding to 1 eV secondary ions. From the negligible slope of the integrated signal between the two bands, it can be concluded that large-angle scattered charge-exchange ion intensities associated with laboratory ion energies exceeding 1 eV are negligible at this energy. At energies below 5 eV, the signal between the two main bands becomes significant.

The good agreement between attenuation and TOF measurements over most of the examined ion energy range indicates that discrimination losses are not important in the present experiments. The accuracy of the present experimental cross sections is estimated at $\pm 20\%$. The present measurements compare favorably with those by Okuno *et al.*,[16] Kushnir *et al.*,[15] and Galli *et al.*[11] Not shown are the liquid-nitrogen cooled drift-tube measurements by Koizumi *et al.*,[17] which are an extension of the methodology of Okuno *et al.* to collision energies as low as 0.01 eV. These measurements are essentially identical to those plotted for Okuno *et al.* in the energy range of interest in this work. The present measurements are in poor agreement with the results of Dillon *et al.*, and are slightly lower than the measurements of Hishinuma.[10] The present cross sections are also substantially higher than the calculated values of Kimura and Watanabe.[12] Closer inspection of that work, however, suggests a typographical error in their cross section table, where the energy unit is given in electron volts, but most likely should be kilo-electron volts. Sakabe and Izawa have missed this error in their data compilation,[9] and we, therefore, also plot the data by Kimura and Watanabe at the corresponding kilo-electron volt energies, where the calculations are more consistent with the present measurements.

An excellent agreement is found between the present cross sections and our semiclassical calculations using the spin-orbit potentials published by Wadt,[36] as seen in Fig. 2 (solid line). The calculated values correspond to the spin-orbit averaged cross sections [Eq. (9)]. More recent Xe_2^+ potentials exist, for which we have also conducted semiclassical calculations. In Fig. 4, calculations based on the potentials of Daskalopoulou *et al.*[35] and Amarouche *et al.*[34] are compared to those based on the Wadt potentials, which are representative of our measurements. The semiclassical calculations are also compared to predictions of the Rapp and Francis model,[6] the presently corrected 1-electron model based on Eq. (15), and the calculations of Sakabe and Izawa,[9] which are based on a time-dependent approach using the LCAO approximation and assuming straight-line trajectories. Note that the measurements are substantially higher than the Rapp and Francis model prediction. The present 1-electron model lies only slightly below the present measurements, which lie closest to the calculations based on the Wadt potentials.

The calculations depend on a good exponential fit of the long-range exchange interactions determined from the charge-exchange potential pair differences. Except for the analytical expressions for the spin-orbit free potentials provided by Amarouche *et al.*,[34] the existing potential data is sparse at long-range, the critical area with respect to charge exchange at low ion energies. Consequently, the present calculations are expected to be most accurate at the highest energies, where the cross section determining impact parameters are the lowest. Table I lists the parameters A and a [Eq. (12)] derived from the potentials of Wadt, Amarouche *et al.*, and Daskalopoulou *et al.* For the latter, we performed fits to Morse potentials except for the Σ_g potential, where we per-

TABLE I. Exchange interaction parameters, A and a [Eq. (12)] derived from the listed Xe_2^+ potentials and used in the calculations of Fig. 5. R specifies the range of interatomic distances at which a good exponential fit was obtained. Values are in atomic units (1 a.u.=27.21 eV=0.529 Å).

Calculation	(u,g) pair	A	a	R
Wadt[a]	$I(1/2)$	22.74	0.901	7–20
	$I(3/2)$	10.28	0.982	7–20
	$II(1/2)$	2.269	0.728	7–20
Amarouche *et al.*[b]	Σ	3.306	0.691	11–20
	Π	3.065	0.977	8–11
		0.154	0.677	10–13
		0.040	0.562	12–15
Daskalopoulou *et al.*[c]	Σ	7.796	0.714	11–28
	Π	3.633	0.839	7.5–22
	$I(1/2)$	4.732	0.711	11–28
	$I(3/2)$	3.633	0.839	7.5–22
	$II(1/2)$	1.523	0.692	9.5–28

[a]See Ref. 36.
[b]See Ref. 34.
[c]See Ref. 35.

TABLE II. Comparison of spin-orbit state cross section ratios, $\sigma_{1/2}/\sigma_{3/2}$, determined experimentally and theoretically.

	Ion energy (LAB, eV)	$\sigma_{1/2}/\sigma_{3/2}$
Johnson (theor)[a]	300	0.86
Hishinuma (exp)[b]	300	0.82 ± 0.04
Kimura (theor)[c]	400	0.9
Wadt[d,e]	300	1.12
	2.6	1.22
Amarouche *et al.*[d,f]	300	1.08
	2.6	1.05
Daskalopoulou *et al.*[d,g]	300	0.97
	2.6	1.03
Present (exp)	300	0.81 ± 0.18
	2.6	0.72 ± 0.23

[a]See Ref. 43.
[b]See Ref. 10.
[c]See Ref. 12.
[d]Present semiclassical calculations based on respective potentials.
[e]See Ref. 36.
[f]See Ref. 34.
[g]See Ref. 35.

formed a fit to the repulsive analytical form used by Amarouche *et al.*[34] The exponentials were then fit to the difference potentials of the derived analytical expressions. The Π exchange energies derived from the Amarouche potentials did not readily fit to an exponential, and fits to three interatomic distance ranges had to be made to optimize for specific energy ranges. All other exchange energies provided high-quality fits to exponentials at the pertinent interatomic distances.

While the potentials of Wadt and Daskalopoulou *et al.* are *ab initio* potentials, those published by Amarouche *et al.* are semi-empirical potentials based in part on the *ab initio* potentials of Michels *et al.*[42] who did not explicitly calculate interaction energies at long range. It is difficult to gauge the quality of the potentials in the critical long-range area from the traditional short-range parameters, D_e and R_e, derived by these authors. The semi-empirical potentials of Amarouche *et al.* exhibit the best agreement with the experimentally determined potential parameters. Daskalopoulou *et al.*,[35] however, have used the most sophisticated methodology (MRD–CI) and the most extensive basis set. All of the spin-orbit potentials are based on the Cohen-Schneider[37] transformation (see Sec. III).

Except for the calculations based on the Wadt potentials, all of the calculations exhibit at low energies cross sections that are higher than the present measurements. This is consistent with significant yields of charge exchange ions with laboratory energies exceeding the blocking potential. The more significant discrepancy between the different calculations at low energy can certainly be attributed to the higher uncertainty of the weak exchange energies at large interatomic distances. At the common Hall thruster acceleration energy of 300 eV, the measurements as well as the present calculations all lie within 50 and 60 Å^2.

The quality of the applied exchange energies can be further checked by comparing the calculated spin-orbit state-selected cross sections with previous results. This is shown in Table II. The only measurements known to us are those by Hishinuma[10] who have determined a $^2P_{1/2}/^2P_{3/2}$ charge exchange cross section ratio of 0.82 ± 0.04 at 300 eV. Johnson[43] calculated similar spin-orbit state-selected cross section ratios using Eqs. (10) and (11) and approximate spin-orbit free exchange energies based on a one-electron approach proposed by Firsov[44] and Smirnov.[45] The estimated Σ and Π exchange interactions used by Johnson result in spin-orbit averaged cross sections that are approximately 20% lower than the present measurements at 300 eV. The semiclassical cross sections based on the three sets of spin-orbit potentials used in the present work generally predict state-selected cross sections that are higher for the excited $^2P_{1/2}$ state, except for the calculation at 300 eV using the potentials of Daskalopoulou *et al.* To ensure that Eqs. (7) and (8) represent a correct approach, we have also conducted calculations with the exchange energies used by Johnson and obtain spin-orbit state-selected cross section ratios close to those determined by Johnson.

Table II also includes measurements taken in our laboratory by comparing the cross sections obtained with electron energies of ~12.1 and 15 eV. At the former electron energy, the electron energy resolution of ~0.5 eV (FWHM) of our experiment permits a near pure production of $^2P_{3/2}$ ions. Assuming a statistical spin-orbit population ratio produced with 15 eV electrons, the spin-orbit cross section ratio is given by

$$\sigma_{1/2}/\sigma_{3/2}=[3\sigma(15)-2\sigma(12.1)]/\sigma(12.1). \quad (16)$$

The measurements, subject to considerable errors, are fully consistent with the earlier measurement and agree with the calculations of Johnson. We thus conclude that potentials with a higher degree of optimization at long range are necessary to correctly reproduce the observed spin-orbit cross-section ratios, thus providing low-energy cross sections with higher confidence levels.

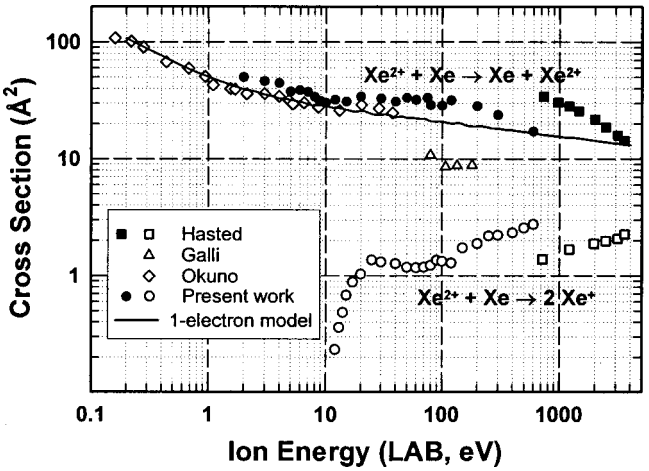

FIG. 5. $Xe^{2+}+Xe$ symmetric and asymmetric charge-exchange cross sections as a function of laboratory ion energy. The present measurements (open and closed circles) are compared with previous experimental work and semiclassical calculations based on a simple 1-electron model of the exchange energy (solid line).

B. $Xe^{2+}+Xe$

Guided-ion beam measurements of the symmetric (double-electron) charge exchange cross sections and the asymmetric single-electron transfer process

$$Xe^{2+}+Xe \rightarrow Xe+Xe^{2+} \tag{17}$$

$$\rightarrow Xe^{+}+Xe^{+} \tag{18}$$

are shown in Fig. 5 and are compared to the existing measurements of Hasted and Hussain,[18] Okuno *et al.*,[16] and Galli *et al.*[11] As for the singly-charged system, the measurements of Koizumi *et al.*[17] are in good agreement with those of Okuno *et al.* The present SCX measurements were obtained with the attenuation method using a 1 eV blocking potential. Consequently, the attenuation experiments discriminate with respect to 2 eV LAB doubly-charged ions and 1 eV LAB singly-charged ions. Sample TOF measurements are ~30% lower than the attenuation measurements. For the present measurements, the estimated error is ±30%.

The attenuation measurements initially provide a total cross section. The SCX cross section is then the difference between the total cross section and the cross section for process (18), which is determined from mass spectrometric analysis of the scattered ion beam. As verified by TOF measurements, the non-symmetric process (18) produces two singly-charged xenon ions: one at velocities near the primary and one near the target gas velocity. Proper ion collection is verified by the observation of equal intensities of the fast and slow product signal components.

The present SCX measurements are slightly higher than previous drift tube measurement by Okuno *et al.*[16] at low energies and approximately 50% lower than the high-energy measurements of Hasted and Hussain in the overlapping energy region. The measurements by Galli *et al.*[11] are significantly lower than all other measurements. The present work is also compared to the corrected 1-electron model assuming an ionization energy of 33.15 eV, the Xe^{2+} 2-electron recombination energy. The approach produces cross sections that are slightly lower than the measurements, but correctly reproduce the cross section energy dependence except for the highest energies. There, competition with the asymmetric channel can explain a steeper drop off with energy. Interestingly, the simple present model is in excellent agreement with the drift tube measurements. In particular, the energy dependence at the lowest energies, governed by the capture cross section which is particularly large due to the q^2 dependence of the long-range ion-induced dipole interaction, is accurately reproduced. The calculation assumes curved trajectories and sets $P(b)=0.5$ [Eq. (4)] for impact parameters below the capture impact parameter. The latter is identified as the lowest impact parameter for which a turning point is defined for the respective purely attractive potential [Eq. (12)].[26]

The asymmetric process (18) has been investigated at thermal energies in ICR[46] and flow tube experiments.[47] While Köding and Nibbering observed a branching ratio of 0.47 for the single-electron process at a total rate coefficient of $3.4\times10^{-9}\,cm^3\,mol^{-1}\,s^{-1}$, Johnsen and Biondi[47] report a rate coefficient for single-electron transfer of $<3\times10^{-14}\,cm^3\,mol^{-1}\,s^{-1}$. The present measurements are fully consistent with the latter study. Measurable cross sections are only observed at laboratory ion energies above 10 eV. As pointed out by Johnsen and Biondi, this is reasonable from a mechanistic point of view because single-electron transfer is purported to occur via a radiative transition at low energies. At higher energies, nonadiabatic transitions overcome the energy gap associated with avoided crossings between the reactant and Coulombic product potential curves. The structure in the present cross sections can be interpreted as stemming from multiple crossings, both associated with different entrance potentials of the reactants and with different reactant states. Recall, that the applied ion source electron energy of 40 eV can produce Xe^{2+} in the metastable ^1D and ^1S states. The present cross sections above 400 eV are approximately twice those measured by Hasted and Hussain.[18] This may be attributed to the superior ion collection efficiencies of the present GIB apparatus.

V. CONCLUSIONS

We present SCX cross sections for singly-charged xenon ions that are in good agreement with semiclassical calculations based on available Xe_2^+ potentials. The current attenuation measurements represent cross sections for producing <1 eV LAB ions, and are thus expected to be smaller than the true SCX cross sections (as observed, for example, in an isotopically resolved experiment) at ion energies below 10 eV. The cross sections are substantially higher than the Rapp and Francis model[6] predictions and lower than the calculations by Sakabe and Izawa[9] except at the lowest energies. The attenuation measurements of the doubly-charged system represent cross sections for producing <2 eV LAB ions. The $Xe^{2+}+Xe$ SCX cross sections are within experimental uncertainties (30%) in good agreement with previous low-energy measurements by Okuno *et al.*[16] and slightly lower than the measurements of Hasted and Hussain[18] at high energies. The

TABLE III. Parameters A and B of Eq. (19) that best fit the present SCX cross section measurements (energy unit: eV).

	A (Å^2)	B (Å^2)
$Xe^+ + Xe$	87.3 ± 0.9	13.6 ± 0.6
$Xe^{2+} + Xe$	45.7 ± 1.9	8.9 ± 1.2

Rapp and Francis model, corrected with respect to the expression for the exchange interaction,[6,26] provides a reasonable estimate of the SCX cross section energy dependence for the $Xe^{2+} + Xe$ system. We are not aware of previous application of this model to multiply-charged SCX systems. The excellent agreement suggests that good first estimates for other SCX systems of multiply charged rare-gas systems including Coulomb collisions, which are much harder to measure, could be obtained using this simple approach. Thus, a comprehensive set of cross sections including higher charge states could be obtained for electrostatic thrusters where charge states as high as $q=4$ have shown to be present in the plasma.[21] Future studies will further test this simple approach by comparing with calculations based on exchange energies obtained by state-of-the-art quantum chemical theory.

The asymmetric $Xe^{2+} + Xe$ system (process 18) exhibits threshold-like behavior with an onset near 10 eV. At a nominal energy of 600 eV, a cross section of 2.8 ± 0.9 Å^2 is observed. The magnitude of this cross section could explain anomalously high energies observed in Hall thruster chamber measurements.[21] Meanwhile, our current investigations of the optical emissions of Hall thruster discharges and plumes find that this process is most likely the source of prominent visible lines useful for diagnostic purposes.

For the thruster modeling community, it is useful to provide a functional form of the present cross sections. The SCX cross sections can be fit to the functional form

$$\sigma^{\mathrm{SCX}} = A - B \log(E). \tag{19}$$

Values of A and B based on the present study are given in Table III. The indicated errors are the statistical standard deviations. Note that the $Xe^{2+} + Xe$ SCX cross sections exhibit some structure in the energy dependence that we cannot fully attribute to experimental artifacts. The energy dependence of the cross sections for process (18) is too structured to be described by a simple functional form.

ACKNOWLEDGMENTS

This work is supported by AFOSR under task No. 2303EP02 (Program Manager: M. Berman) and was performed while the author J. S. M. held a National Research Council-Air Force Research Laboratory Associateship. The authors are also indebted to Dr. Mitat Birkan of AFOSR for additional support. The authors thank Iain D. Boyd, Art Phelps, and Edmond Murad for many helpful comments.

[1] M. G. Marcucci and J. E. Polk, Rev. Sci. Instrum. **71**, 1389 (2000).
[2] J. E. Polk, J. R. Brophy, and J. Wang, *AIAA 95-2924, 31st AIAA/ASME/SAE/ASEE Joint Propulsion Conference and Exhibit* (San Diego, CA, 1995).
[3] R. I. Samanta Roy, D. E. Hastings, and N. A. Gatsonis, J. Spacecr. Rockets **33**, 525 (1996).
[4] R. I. Samanta Roy, D. E. Hastings, and S. Taylor, J. Comp. Phys. **128**, 6 (1996).
[5] J. Wang, D. Brinza, R. Goldstein, J. Polk, and M. Henry, *AIAA 99-3734, 30th Plasmadynamics and Lasers Conference*, Vol. 99-3734 (Norfolk, VA, 1999).
[6] D. Rapp and W. E. Francis, J. Chem. Phys. **37**, 2631 (1962).
[7] I. Boyd, J. Propul. Power **16**, 902 (2000).
[8] M. W. Crofton and I. D. Boyd, J. Propul. Power **17**, 203 (2001).
[9] S. Sakabe and Y. Izawa, At. Data Nucl. Data Tables **49**, 257 (1991).
[10] N. Hishinuma, J. Phys. Soc. Jpn. **32**, 1452 (1972).
[11] A. Galli, A. Giardini-Guidoni, and G. G. Volpi, Nuovo Cimento **26**, 846 (1962).
[12] M. Kimura and T. Watanabe, J. Phys. Soc. Jpn. **31**, 1600 (1971).
[13] J. A. Dillon, W. F. Sheridan, H. D. Edwards, and S. N. Gosh, J. Chem. Phys. **23**, 776 (1955).
[14] B. I. Kikiani, Z. E. Saliya, and I. B. Bagdasarova, Sov. Phys. Tech. Phys. **20**, 364 (1975).
[15] R. M. Kushnir, B. M. Palyukh, and L. A. Sena, Bull. Acad. Sci. USSR, Phys. Ser. (Engl. Transl.) **23**, 995 (1959).
[16] K. Okuno, T. Koizumi, and Y. Kaneko, Phys. Rev. Lett. **40**, 1708 (1978).
[17] T. Koizumi, K. Okuno, N. Kobayashi, and Y. Kaneko, J. Phys. Soc. Jpn. **51**, 2650 (1982).
[18] J. B. Hasted and M. Hussain, Proc. Phys. Soc. **83**, 911 (1964).
[19] I. P. Flaks and E. S. Solov'ev, Sov. Phys. Tech. Phys. **3**, 564 (1958).
[20] L. B. King and A. D. Gallimore, Phys. Plasmas **6**, 2936 (1999).
[21] L. B. King and A. D. Gallimore, J. Propul. Power **16**, 916 (2000).
[22] H. S. W. Massey and H. B. Gilbody, *Electronic and Ionic Impact Phenomena*, 2nd ed. (Oxford University Press, London, 1974), Vol. 4.
[23] E. Teloy and D. Gerlich, Chem. Phys. **4**, 417 (1974).
[24] D. Gerlich, Adv. Chem. Phys. **82**, 1 (1992).
[25] E. E. Ferguson, F. C. Fehsenfeld, and A. L. Schmeltekopf, Adv. At. Mol. Phys. **5**, 1 (1969).
[26] S. H. Pullins, R. A. Dressler, R. Torrents, and D. Gerlich, Z. Phys. Chem. (Munich) **214**, 1279 (2000).
[27] F. X. Gadea and I. Paidarová, Chem. Phys. **209**, 281 (1996).
[28] R. A. Dressler, R. H. Salter, and E. Murad, J. Chem. Phys. **99**, 1159 (1993).
[29] M. J. Bastian, R. A. Dressler, D. J. Levandier, E. Murad, F. Muntean, and P. B. Armentrout, J. Chem. Phys. **106**, 9570 (1997).
[30] A. A. Radzig and B. M. Smirnov, *Reference Data on Atoms, Molecules, and Ions*, Springer Series in Chem. Phys. Vol. 31 (Springer, Berlin, 1985).
[31] P. Bolognesi, S. J. Cavanagh, L. Avaldi, R. Camilloni, M. Zitnik, M. Stuhec, and G. C. King, J. Phys. B **33**, 4723 (2000).
[32] H. S. W. Massey and R. A. Smith, Proc. R. Soc. London, Ser. A **142**, 142 (1933).
[33] F. J. Smith, Physica (Amsterdam) **30**, 497 (1964).
[34] M. Amarouche, G. Durand, and J. P. Malrieu, J. Chem. Phys. **88**, 1010 (1988).
[35] M. Daskalopoulou, H.-U. Böhmer, and S. D. Peyerimhoff, Z. Phys. D: At., Mol. Clusters **15**, 161 (1990).
[36] W. R. Wadt, J. Chem. Phys. **68**, 402 (1978).
[37] J. S. Cohen and B. Schneider, J. Chem. Phys. **61**, 3230 (1974).
[38] R. E. Johnson, J. Phys. D **3**, 539 (1970).
[39] R. P. Marchi and F. T. Smith, J. Chem. Phys. **139**, 1025 (1965).
[40] K. T. Tang, J. P. Toennies, and C. L. Yiu, J. Chem. Phys. **94**, 7266 (1991).
[41] T. C. Scott, J. F. Babb, A. Dalgarno, and J. D. Morgan, J. Chem. Phys. **99**, 2841 (1993).
[42] H. H. Michels, R. H. Hobbs, and L. A. Wright, J. Chem. Phys. **69**, 5151 (1978).
[43] R. E. Johnson, J. Phys. Soc. Jpn. **32**, 1612 (1972).
[44] O. Firsov, Zh. Eksp. Teor. Fiz. **21**, 1001 (1951).
[45] B. M. Smirnov, Sov. Phys. JETP **20**, 345 (1965).
[46] H. von Köding and N. M. M. Nibbering, Int. J. Mass. Spectrom. **185/186/187**, 281 (1999).
[47] R. Johnsen and M. A. Biondi, Phys. Rev. A **20**, 87 (1979).